Optimization of an Optical Fiber Drawing Process under Uncertainty

ARTICLE *in* INDUSTRIAL & ENGINEERING CHEMISTRY RESEARCH · MAY 2006

Impact Factor: 2.59 · DOI: 10.1021/ie060045u

7 AUTHORS, INCLUDING:

Luke Achenie
Virginia Polytechnic Institute and State Univ…
127 PUBLICATIONS **1,261** CITATIONS
SEE PROFILE

Eugene Santos
Dartmouth College
212 PUBLICATIONS **1,400** CITATIONS
SEE PROFILE

Optimization of an Optical Fiber Drawing Process under Uncertainty

Charles Acquah,[†] Ivan Datskov,[†] Andryas Mawardi,[‡] Feng Zhang,[§] Luke E. K. Achenie,*[,†] Ranga Pitchumani,[‡] and Eugene Santos[§,||]

Departments of Chemical Engineering, Mechanical Engineering, and Computer Science and Engineering, 191 Auditorium Road, Unit 3222, University of Connecticut, Storrs, Connecticut 06269

Optical fibers are used in diverse applications ranging from ocean and terrestrial cables to remote sensors and to light guides in medical applications. The information and telecommunications industries are other fields where optical fibers are actively used. However, the full potential of optical fibers has not been realized because of performance and production limitations. In the manufacturing process, high draw speeds result in large temperature gradients, which often lead to inferior quality fiber with poor optical and mechanical properties. On the other hand, low draw speeds lead to superior quality fiber with better optical and mechanical properties. Here, quality is achieved at the expense of a reduced rate of production. Therefore, the realization of good quality fiber without unduly compromising the production throughput can be assessed through the solution of an optimization model. The objective is to maximize the fiber draw speed subject to constraints on fiber mechanical and transmission properties. Additional complications arise in the optimization problem when uncertainties in process and model parameters are accounted for.

1. Introduction

Optical fibers are used in a considerable number of applications ranging from ocean and terrestrial cables to remote sensors and to light guides in medical and other applications. They have also found wide usage in the information and communications industry. Because of the increased demand on bandwidth for transmitting large volumes of information faster, cheaper, and more reliably, manufacturing high-quality optical fibers that will guarantee reliability in performance at high production levels deserves much attention. In the manufacturing process, high fiber draw rates often result in inferior quality fiber with poor mechanical properties. On the other hand, low draw speeds lead to superior quality fiber with better mechanical properties at the expense of decreased rate of production. The realization of good quality fiber without unduly compromising the production throughput is accomplished through the solution of an optimization model. Naturally, since there are significant uncertainties in process and model parameters, there is a need to account for them in the optimization model.

Accounting for uncertainty in chemical process design has been an area of active research in the past few years. Most engineering processes and designs are based on models having parameters which take on nominal values. However, in real time, processes fluctuations abound. These variabilities arise because of varying process conditions (e.g., temperature instabilities) and inaccuracies in the experimental determination of model parameters (e.g., energy of activation, diffusion constants, and viscosity parameters). Hence, for a process to remain feasible (all process constraints are satisfied) at the operation stage, it is imperative that the effects of uncertainties are accounted for at the design stage. Infeasibilities during the operational stage lead to suboptimal and poor quality products. There are some instances where safety is a major concern. For instance, Rooney and Biegler[1] have shown that failure to consider uncertainty in the design of a flexible pressure relief valve could lead to a large pressure increase and possible explosion. A vast majority of the work done in the area of design under uncertainty has focused on systems where the cost function and constraints are analytic in nature.[1−10] However, uncertainty considerations in processes where the cost function and constraints are nonanalytic has received very little attention. The optical fiber fabrication process falls under this category. These processes are governed by a highly nonlinear system of partial differential-algebraic equations (DAE). Given inputs to the DAE model, outputs of interest are generated and used in computing the objective function and constraints needed in the optimization problem.

The objective is to maximize the fiber draw speed subject to constraints on fiber mechanical (e.g., defects, residual stress, and drawing tension) and transmission (e.g., refractive index profile) properties while simultaneously taking into account uncertainties in process and model parameters. Because of the nonlinearities inherent in the fiber drawing model, the objective function and constraints also turn out to be nonlinear. The fiber drawing optimization problem is thus formulated as a nonlinear programming (NLP) problem. The split-and-bound (SB)[11] method for solving the two-stage optimization problem (TSOP) under uncertainty has been adapted for the fiber drawing problem. The SB method uses sequential quadratic programming (SQP), which is a local optimizer, for solving the various NLP subproblems. In view of this, optimization runs are carried out using multiple initial guesses of the decision variables in order to guarantee a near-global optimal solution.

This paper systematically studies (1) the effect of uncertainty on fiber draw speed and (2) the effect of constraints on fiber draw speed. The production throughput, which is related to the fiber draw velocity, will be used as a measure of the process performance. The study of the effect of uncertainty on fiber draw speed therefore gives much insight into what represents an acceptable compromise on the fiber draw speed in the presence of uncertainties. Finally, the study of the effect of constraints on the fiber draw speed is necessary, since this provides information as to what is an acceptable deviation from

* To whom correspondence should be addressed. E-mail: achenie@engr.uconn.edu.

[†] Department of Chemical Engineering.

[‡] Department of Mechanical Engineering.

[§] Department of Computer Science and Engineering.

[||] Current address: Eugene Santos Jr. Thayer School of Engineering, Dartmouth College, 8000 Cummings Hall, Hanover, NH 03755.

10.1021/ie060045u CCC: $33.50
Published on Web 05/10/2006

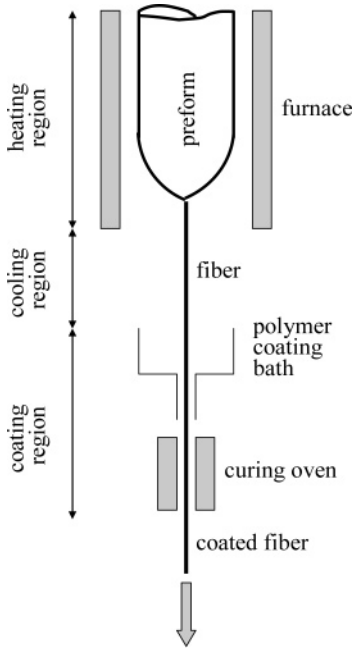

Figure 1. Schematic of the optical fiber drawing and coating process.

the optimal refractive index profile in order to track the optimum fiber draw speed as closely as possible.

The paper is organized as follows: Section 1 introduces the field of optical fibers and a few application areas. It also touches on the need to account for uncertainties during the manufacturing process. A description of the optical fiber process model is given in Section 2. Section 3 presents the formulation of the fiber drawing optimization problem under uncertainty. Section 4 briefly outlines the SB−TSOP solution strategy adapted for solving the fiber drawing problem. This is followed by discussion of results in Section 5. The summary and conclusions of this work are given in Section 6.

2. Brief Description of the Optical Fiber Drawing Process

The schematic of the fiber drawing process is shown in Figure 1. The optical fiber is produced by a continuous drawing process with basically three main regions: heating, cooling, and coating.

The input material to the fiber drawing process is a solid preform made of silica glass. This is fabricated separately using a modified chemical vapor deposition (MCVD) process,[12] a description of which is outside the scope of this paper. In the heating region, the solid preform rod is heated to melting. The softened glass preform is drawn in the axial direction under tension. During the drawing process, materials referred to as dopants are often added to the preform to either enhance or decrease the refractive index of the resulting fiber. Materials such as germanium(IV) oxide (GeO_2) and phosphorus pentaoxide (P_2O_5) increase the refractive index of the pure silica, whereas boron oxide (B_2O_3) decreases the refractive index. The fiber exiting from the furnace has a relatively flawless surface, which is characteristic of high strength. The fiber is then drawn through a polymer bath, where it gathers a thin coating layer that gets solidified by a cross-linking process usually referred to as cure. Coating is necessary to protect the fiber from external damage. The final fiber product is then wound on take-up reels under a given tension during the drawing process.

Modeling the fiber draw process requires a physical description of the governing transport phenomena (thermal, diffusion, and radiation) in all three regions. Several researchers have carried out extensive studies in this area.[13−21] The focus has been on investigating various transport mechanisms, including heat transfer in the heating region, extensional flow of the softened glass preform and evolution of the neck-down profile. Modeling the coating region has also been reported in the literature with emphasis directed toward predicting coating thickness and energy requirements for ultraviolet-radiation-based curing of the coating layer.[22−26] It is worth mentioning that the focus of this paper is not on the numerical simulation of the fiber drawing process. This paper specifically addresses the optimization of the fiber drawing process under uncertainty using an optical fiber numerical model developed by Yan and Pitchumani.[27] A summary of process description and governing equations for mass (eq 1), momentum (eqs 2 and 3), energy (eq 4), and transport (eq 5) is hereby given. All terms are defined in the nomenclature.

$$\frac{\partial \rho u}{\partial z} + \frac{1}{r}\frac{\partial (rv)}{\partial r} = 0 \tag{1}$$

$$\frac{\partial (\rho u^2)}{\partial z} + \frac{1}{r}\frac{\partial (\rho ruv)}{\partial r} = -\frac{1}{\rho}\frac{\partial p}{\partial z} + 2\frac{\partial}{\partial z}\left(\mu \frac{\partial u}{\partial z}\right) + \frac{1}{r}\frac{\partial}{\partial r}\left[r\mu\left(\frac{\partial u}{\partial r} + \frac{\partial v}{\partial r}\right)\right] \tag{2}$$

$$\frac{\partial (\rho uv)}{\partial z} + \frac{1}{r}\frac{\partial (\rho r v^2)}{\partial r} = -\frac{1}{\rho}\frac{\partial p}{\partial z} + \frac{\partial}{\partial z}\left[\mu\left(\frac{\partial u}{\partial r} + \frac{\partial v}{\partial r}\right)\right] + \frac{2}{r}\frac{\partial}{\partial r}\left[r\mu\left(\frac{\partial v}{\partial r}\right)\right] - \frac{2\mu v}{r^2} \tag{3}$$

$$\frac{\partial (\rho C_p uT)}{\partial z} + \frac{1}{r}\frac{\partial (\rho C_p rvT)}{\partial r} = \frac{\partial}{\partial z}\left(K\frac{\partial T}{\partial z}\right) + \frac{1}{r}\frac{\partial}{\partial r}\left(rK\frac{\partial T}{\partial r}\right) + \mu\left\{2\left[\left(\frac{\partial u}{\partial r}\right)^2 + \left(\frac{u}{r}\right)^2 + \left(\frac{\partial v}{\partial z}\right)^2\right] + \left(\frac{\partial u}{\partial z} + \frac{\partial v}{\partial r}\right)^2\right\} \tag{4}$$

$$\frac{\partial (uc)}{\partial z} + \frac{1}{r}\frac{\partial (rvc)}{\partial r} = \frac{\partial}{\partial z}\left(D\frac{\partial c}{\partial z}\right) + \frac{1}{r}\frac{\partial}{\partial r}\left(rD\frac{\partial c}{\partial r}\right) \tag{5}$$

The fiber model makes the assumptions that the neck-down profile is known and also that the flow and temperature field is not significantly affected by the dopant. The velocity across the interface of the preform/fiber and inert gas is zero while the velocity along the interface is continuous on both sides of the interface. This velocity is obtained by applying a no-shear boundary condition to the preform/fiber at the interface. In the drawing region, temperature is continuous, and the heat flux satisfies the following condition:

$$\left(k\frac{\partial T}{\partial n}\right)_{\text{fiber}} = \left(k\frac{\partial T}{\partial n}\right)_{\text{gas}} + q_{\text{rad}} \tag{6}$$

In the cooling region, a prescribed convection coefficient is applied to the fiber surface at the natural convective cooling region. The surface temperature satisfies the following equation, which is also used as a boundary condition,

$$\frac{\partial \theta}{\partial R} = Bi(\theta_\infty - \theta) \tag{7}$$

where Bi is the Biot number (assumed to be a constant in the range 150−300 W/(m^2 K)) for natural convection. The governing equations together with boundary conditions are solved using a control volume finite difference method. For the flow and temperature fields, three regions, namely, drawing, natural cooling, and forced cooling, are considered. Each region is solved separately, and temperature at the junctions is compared

until convergence. For the dopant concentration filed, only two regions made up of drawing and cooling are considered. Here, each region is solved separately, and concentration at the interface is compared until convergence. The velocity and temperature fields are solved for all participants in the drawing and cooling region. The dopant diffusion equation is then solved using the velocity and temperature solutions obtained previously.

Outputs from the numerical simulator are velocity, temperature, pressure, and index of refraction profiles. Further numerical analysis is performed using information from these profiles in conjunction with eqs 8, 9, 10, and 14 to obtain key output variables; namely, velocity, defects, tension, stress, maximum refractive index profile error, and average refractive index profile error are obtained. The velocity is used in computing the objective function, whereas defects, tension, stress, and maximum and average index of refraction profile error are used in the computation of constraints needed in the optimization. The drawing-induced defects[28] can be expressed as

$$n_{\mathrm{def}}(T) = n_{\mathrm{p}} \exp\left(-\frac{E_{\mathrm{f}}}{kT} - \frac{A}{V}\right) \tag{8}$$

where T is the drawing temperature, V is the drawing velocity, A is a constant, and E_{f} is the energy of formation. It can be seen from eq 8 that, by keeping all other terms constant, an increase in temperature results in an increase in the number of defects. The drawing tension,[13] which is a combination of viscous force, surface tension, inertia, and shear force exerted by the external fluid, can be expressed as

$$F_{\mathrm{tens}} = F_{\mu} + F_{\varsigma} + F_{\mathrm{I}} + F_{\mathrm{e}} - F_{\mathrm{g}} \approx 3\eta A \frac{\partial \upsilon}{\partial z} \tag{9}$$

In eq 9, η is the fluid viscosity, A is the cross-sectional area of the fiber core, z is the distance in the axial direction of the fiber, and υ is the axial coordinate velocity. The residual stress induced in fibers is a superposition of thermal stress[29] caused by difference in thermal expansion coefficients between core and cladding and mechanical stress[30] caused by difference in viscosity properties in the two regions.

$$\sigma_z(r) = \sigma_{\mathrm{m}} + \sigma_{\mathrm{t}}(r) \tag{10}$$

The corrected index of refraction profile,[31] which is a relationship between refractive index and stress arising from photoelastic effects, is given by

$$\Delta n_{\mathrm{r}} = C_{\mathrm{a}}\sigma_r + C_{\mathrm{b}}(\sigma_\theta + \sigma_z) \tag{11}$$

$$\Delta n_\theta = C_{\mathrm{a}}\sigma_\theta + C_{\mathrm{b}}(\sigma_z + \sigma_r) \tag{12}$$

$$\Delta n_z = C_{\mathrm{a}}\sigma_z + C_{\mathrm{b}}(\sigma_r + \sigma_\theta) \tag{13}$$

where C_{a} and C_{b} are the photoelastic coefficients of SiO_2. Δn_r, Δn_θ, and Δn_z are the refractive index changes in the radial, circumferential, and axial directions, respectively. σ_r, σ_θ, and σ_z are the radial, circumferential, and axial components of the stress in the core. The refractive index in the radial direction, Δn_r, is considered the most important for propagating light signal in optical fibers. Additionally, for a single-mode fiber core, $\sigma_z \approx \sigma_{1r}$ ($\gg \sigma_r$, σ_θ), consequently eq 11 simplifies to

$$\Delta n_r = C_{\mathrm{a}}\sigma_r + C_{\mathrm{a}}(\sigma_\theta + \sigma_z) \approx C_{\mathrm{b}}\sigma_z \tag{14}$$

3. Formulation of the Fiber Drawing Optimization Problem under Uncertainty

The fiber drawing problem consists of determining the maximum draw speed while satisfying constraints related to fiber mechanical (e.g., defects, residual stress, and drawing tension) and transmission (e.g., refractive index) properties. The optimization is carried out over eight decision variables, namely, furnace wall temperature, cooling disk temperature, initial square profile, initial dopant concentration, furnace length, cooling gas velocity, inert gas velocity, and fiber draw velocity. These variables are operating parameters that directly impact the fiber drawing process. Additional complications arise in the optimization when uncertainties are accounted for.

Table 1. Notation and Nominal Values for Uncertain Parameters[a]

θ	uncertain parameter	notation	nominal value	units
θ_1	temperature of furnace wall	T_{w}	$2.37 \times 10^{+3}$	K
θ_2	temperature of cooling disc	T_{d}	$2.92 \times 10^{+2}$	K
θ_3	viscosity parameter, 1	vis1	1.26×10^{-14}	Ns m^{-2}
θ_4	viscosity parameter, 2	vis2	$3.20 \times 10^{+4}$	K
θ_5	inert diffusion constant, 1	D_0	1.87×10^{-6}	m^2 s^{-1}
θ_6	inert diffusion constant, 2	D_1	$3.34 \times 10^{+4}$	K
θ_7	radiation parameter, 1	rad1	$4.00 \times 10^{+2}$	m^{-1}
θ_8	radiation parameter, 2	rad2	$1.50 \times 10^{+4}$	m^{-1}

[a] Note: vis1 and vis2 have different units. Likewise D_0 and D_1 have different units. Refer to eqs 15 and 16 to see context.

Two groups of uncertain parameters, process and model parameter uncertainty, are considered (see Table 1). The uncertain parameter vector is represented by θ. Processing conditions such as the furnace wall temperature and cooling disk temperature are considered uncertain. This is due to the fact that, in practice, temperature is subject to control fluctuations. In addition, the viscosity, diffusion and radiation coefficients used in the fiber numerical model are considered uncertain, reflecting inaccuracies that exist in their empirical determination. The form of the diffusion coefficient in the numerical model follows the Arrhenius relation. Here, D is the diffusion coefficient, D_0 and D_1 are inert diffusion constants, and T is the physical temperature in Kelvin (K).

$$D = D_0\, \mathrm{e}^{-(D_1/T)} \tag{15}$$

Similarly, the viscosity coefficient, V_η, is modeled using an Arrhenius-type relation. T is the physical temperature in Kelvin (K) and vis1 and vis2 are viscosity parameters.

$$V_\eta = \mathrm{vis1}\, \mathrm{e}^{-(\mathrm{vis2}/T)} \tag{16}$$

In the fiber drawing problem, five constraints are imposed. These constraints are necessary to maintain integrity of the final optical fiber produced. Three of the five constraints relate to mechanical strength, while the other two relate to deviation of the actual refractive index profile from the target profile. As a first constraint, the number of defects, n_{def}, in the final fiber must not exceed a fixed critical number of defects, $n_{\mathrm{def,crit}}$.

There are also constraints on the drawing tension, F_{tens}, and the processing-induced residual stress, σ_{res}, of the fiber. For instance, σ_{res} within the fiber must not exceed a critical value, $\sigma_{\mathrm{res,crit}}$, to prolong fiber life and performance. Finally, two more constraints are placed on the maximum and average value of the normalized difference between actual and target refractive index profiles. The constraints on the index of refraction profile error are necessary to ensure that the optical transmission properties (e.g., the refractive index) match specified values. An illustration of the reference and actual refractive index profiles is shown in Figure 2. A half-circle is used as the reference profile. The maximum index of refraction profile error,

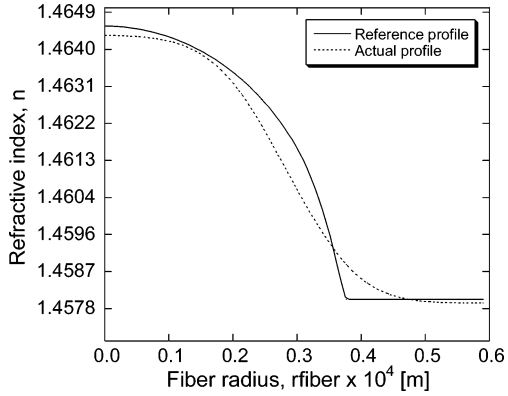

Figure 2. Plot of refractive index versus fiber radius showing the actual and reference profiles.

n_{max} , and the average index of refraction profile error, n_{avg}, are computed using eqs 17 and 18, respectively,

$$n_{max} = \max|(n_{actual} - n_{ref})| \tag{17}$$

$$n_{avg} = \frac{1}{R}\int_0^R |(n_{actual} - n_{ref})|\, dr \tag{18}$$

where n_{actual} and n_{ref} are the actual and reference refractive indices, respectively, and R is the radius of the fiber core, which is taken to be 5.9×10^{-5} m in the numerical model.

In the TSOP formulation for solving design problems under uncertainty, the objective function is evaluated as an expected (mean) value, whereas the constraints are treated deterministically for each realization of θ within the domain of the uncertain parameter, T^{θ}. As explained earlier, the fiber drawing optimization problem is posed as a multiperiod nonlinear programming problem (NLP) and is written mathematically as

$$\underset{T_w,T_d,r_a,c_i,u_0,u_g,z_L,V}{\text{Maximize}} E_{T\theta}(V) \tag{19}$$

Subject to:

$$\mathbf{g}_1 = n_{def}(\mathbf{d}^k, \mathbf{z}^i, \boldsymbol{\theta}^i) - n_{def,crit} \le 0 \tag{20}$$

$$\mathbf{g}_2 = F_{tens}(\mathbf{d}^k, \mathbf{z}^i, \boldsymbol{\theta}^i) - F_{tens,crit} \le 0 \tag{21}$$

$$\mathbf{g}_3 = \sigma_{res}(\mathbf{d}^k, \mathbf{z}^i, \boldsymbol{\theta}^i) - \sigma_{res,crit} \le 0 \tag{22}$$

$$\mathbf{g}_4 = \epsilon_{max}(\mathbf{d}^k, \mathbf{z}^i, \boldsymbol{\theta}^i) - \epsilon_{max,crit} \le 0 \tag{23}$$

$$\mathbf{g}_5 = \epsilon_{avg}(\mathbf{d}^k, \mathbf{z}^i, \boldsymbol{\theta}^i) - \epsilon_{max,crit} \le 0 \tag{24}$$

Here, **d** and **z** represent the vectors of design and control variables, respectively. $\mathbf{g}_j$ is the vector of constraints, where j is an index representing the number of constraints.

The index k is an iteration counter, and index i is used to represent the number of approximated points (quadrature points) used for the numerical integration of the objective function. The design and control variables together with the associated design intervals are given in Tables 2 and 3, respectively. The above NLP is solved using the SB−TSOP solution framework, which is discussed briefly in Section 4.

4. SB−TSOP Solution Framework

The two-stage optimization problem (TSOP) formulation is used for solving optimization problems under uncertainty. The two stages represent the initial design stage followed by the operational stage. In the design stage, design variables are selected and are not allowed to change once the plant becomes operational. However, during operation of the plant, another set of variables, referred to as control variables, are adjusted to offset the effect of uncertainties. This ensures that, given any realization of uncertainty, all process constraints will be satisfied. This is the basic idea behind the two-stage strategy for solving design problems under uncertainty. On the other hand, there are situations where there are no control variables or control variables remain constant during plant operation. In this case, the TSOP degenerates into what is generally referred to as a one-stage optimization problem (OSOP).

Table 2. Design Variables and Associated Design Intervals

d	design variables	symbol	design interval
d_1	furnace wall temperature (K)	T_w	$1900 \le T_w \le 2850$
d_2	cooling disk temperature (K)	T_d	$280 \le T_d \le 304$
d_3	initial profile parameter, 1	r_a	$0.05 \le r_a \le 0.95$
d_4	initial profile parameter, 2	c_0	$0.05 \le c_0 \le 0.30$
d_5	furnace length (m)	z_L	$0.25 \le Z_L \le 0.35$
d_6	fiber draw velocity (m/s)	V	$0.50 \le V \le 15.0$

Table 3. Control Variables and Associated Intervals

z	control variables	symbol	interval
z_1	cooling gas velocity (m/s)	u_{cg}	$0.50 \le u_{cg} \le 2.00$
z_2	inert gas velocity (m/s)	u_{ig}	$0.01 \le u_{ig} \le 0.10$

Several approaches, stochastic and deterministic, have been proposed for solving the TSOP. Several researchers[32−40] have used stochastic approaches. Deterministic methods for solving the TSOP have also been reported in the literature.[41−45] In particular, the deterministic SB technique[44] for solving the TSOP under uncertainty will be used for the fiber drawing problem. A summary of the SB algorithm is given as follows:

- Step 1: Set iteration counter $k = 0$ and choose an initial partition of the uncertainty region T into subregions T_i^k ($i = 1, .., N^{(k)}$). Next, choose the set of approximation points S_1 and an initial set of critical points $S_2^{(0)}$. Initialize the design variable vector, $\mathbf{d}^{(0)}$.
- Step 2: Solve upper-bound problem given by eq 25:

$$f^{U,(k)} = \min_d \sum_{i\in S_1} w_i f(\mathbf{d}, \mathbf{z}^i, \boldsymbol{\theta}^i) \tag{25}$$

Subject to:

$$\max_{\theta\in T_i^k} \mathbf{g}_j(\mathbf{d}, \mathbf{z}^i, \boldsymbol{\theta}^i) \le 0, \quad i \in S_1, \quad j = 1, ..., m$$

Let $[\mathbf{d}^{(k)}, f^{U,(k)}]$ be the optimal solution for eq 25.

- Step 3: Determine the set $Q^{(k)}$ of active constraints in the upper-bound problem,

$$\chi_{1i}(\mathbf{d}, \mathbf{z}, \boldsymbol{\theta}) = 0, \quad i \in Q^{(k)} \tag{26}$$

where χ_1 is the feasibility condition given by

$$\chi_1(\mathbf{d}, \mathbf{z}, \boldsymbol{\theta}) = \max_{\theta\in T} \min_{z\in Z} \max_{j\in J} \mathbf{g}_j(\mathbf{d}, \mathbf{z}, \boldsymbol{\theta}) \le 0 \tag{27}$$

- Step 4: If $Q^{(k)}$ is empty, then the solution to the problem is found; stop.
- Step 5: Solve lower-bound problem (eq 28), for set of critical points obtained in Step 3.

$$f^{L,(k)} = \min_d \sum_{i\in S_1} w_i f(\mathbf{d}, \mathbf{z}^i, \boldsymbol{\theta}^i)$$

Subject to:

$$\mathbf{g}_j(\mathbf{d}, \mathbf{z}^i, \boldsymbol{\theta}^i) \leq 0, \quad i \in S_1, \quad j = 1, ..., m$$

$$\mathbf{g}_j(\mathbf{d}, \mathbf{z}^{lq}\boldsymbol{\theta}^{lq}) \leq 0, \quad \forall \boldsymbol{\theta}^{lq} \in S_l^{(k)}, \quad l = 1, ..., N^{(k)} \qquad (28)$$

Let $[\mathbf{d}^{(k)}, f^{\mathrm{L},(k)}]$ be the optimal solution for eq 28.

- Step 6: If $|f^{\mathrm{U},(k)} - f^{\mathrm{L},(k)}| \leq \epsilon$ (ϵ is sufficiently small and positive scalar), then the solution to the original TSOP is found; stop.
- Step 7: If the condition specified in Step 6 is not met, then construct a new set of critical points (points of constraint violation) and update the discretization.
- Step 8: Set $k = k + 1$ and go to Step 2.

The above algorithm is carried out iteratively until a solution is found. If no solution is found, the algorithm terminates with an infeasible solution. In general, there are two ways of handling infeasible solutions. The first approach is to carry out the optimization using random multiple initial guesses of the optimization search variables. A second approach is to observe the direction in which the infeasible solution is heading and to make slight perturbations around the infeasible solution to move the optimization in the direction of a feasible solution. In general, the two approaches were used, but they both invariably make use of a different starting point. Additionally, a fine-grained as opposed to a coarse-grained partition of uncertain parameter space is used. The use of fine-grained partitioning helps in identification of critical points within a given subregion of the uncertainty parameter space but results in a large computational overhead.

5. Results and Discussion

The results obtained from the optimization runs were dependent on the fidelity of the optical fiber numerical process model. Validation of the optical fiber process model has been reported,[27] in which predictions from the numerical model were shown to closely agree with numerical data from the model developed by the Choudhury and Jaluria group.[46,47] Additionally, the use of a local gradient-based SQP method implies that convergence to local minima is expected. An attempt to obtain near-globally optimum solutions was made by carrying out the optimization using multiple initial guesses from within the domain of the design variable vector, and the best solution (in this case, the maximum) from among the several locally optimal solutions was taken as the near-global maximum. All computations were performed using the NCSA high-speed supercomputing resources at the University of Illinois, Urbana-Champaign.

We also carried out a preliminary sensitivity analysis to investigate both the independent and interactive effects of uncertain parameters on the fiber drawing process. For each uncertain parameter, 200 samples were generated from the domain of uncertain parameters using the Latin Hypercube sampling (LHS) technique.[48] An input coefficient of variance of 2.0% was used. Each uncertain parameter is varied, and the others are kept constant. This is to investigate the independent effect of wall temperature on the outputs of interest. A single simulation is then carried out, and the numerical values for defects, stress, tension, maximum error, and average error were computed. The procedure is repeated, and the simulations are carried out for all 200 samples.

The mean, μ, and standard deviation, σ, were calculated. In each case, the coefficient of variance, σ/μ, expressed as a percentage, was computed and used as a measure of spread (Table 4).

Table 4. Sensitivity Analysis for Each Uncertain Parameter

uncertain parameter	symbol	defects (n_{def})	stress (σ_{res})	tension (F_{tens})	max. error (n_{max})	avg. error (n_{avg})
θ_1	T_{w}	0.636	4.125	15.35	6.692	26.43
θ_2	T_{d}	0.002	0.251	0.052	0.017	0.087
θ_3	vis1	0.000	0.113	0.658	0.000	0.001
θ_4	vis2	0.000	2.412	15.37	0.000	0.002
θ_5	D_0	0.000	0.086	0.008	0.227	1.055
θ_6	D_1	0.000	2.151	0.000	8.141	24.76
θ_7	rad1	0.000	0.000	0.000	0.000	0.000
θ_8	rad2	0.000	0.000	0.000	0.000	0.000
θ	combined	0.628	5.539	23.45	9.912	35.90

The results presented in Table 4 clearly indicate that the furnace wall temperature, T_{w}, has the greatest impact on the fiber drawing process, since it affects all outputs of interest, namely, defects, stress, tension, maximum error, and average error, by a large margin. This is so because all the thermophysical properties of fiber are temperature dependent. The cooling disk temperature, T_{d}, affects all output variables but only to a very small extent. The viscosity model parameters, vis1 and vis2, only affect stress and tension. However, the defects, maximum error, and average error output variables are unaffected by the viscosity coefficients. The diffusion constants, D_0 and D_1, do not affect defects, stress, and tension. However, the maximum error and average error are greatly affected by the presence of diffusion. The radiation coefficients, rad1 and rad2, do not affect output variables at a 2.0% input coefficient of variance. The radiation coefficients were still considered as uncertain, since their interactive effect with the other uncertain parameters is unknown. Additionally, it is anticipated that, as the level of uncertainty increases, the effect of radiation could become significant. The last row of Table 4 presents the case where the interactive effects of all uncertain parameters are studied. Clearly, the interactive effect of uncertain parameters is very significant.

This preliminary study using sensitivity analysis provides useful insight into the extent to which uncertainty impacts the fiber drawing process. It also provides information on what represents a realistic maximal level of uncertainty to be used for study in the optimization. To enhance flow during the draw process, the silica preform has to be heated well above the melting temperature, which is taken as 1900 K in the fiber simulation. Suppose a temperature of 2400 K is achieved; then $\sigma/\mu = 5.0\%$ implies a temperature change of 120 K. This represents a big change from the nominal value, resulting in large temperature gradients. Given the tight constraints imposed on the fiber drawing problem, such large temperature gradients often lead to infeasible solutions and impractical designs. As shown previously in Table 4, the maximum refractive index profile error and average refractive index profile error are very sensitive to the furnace wall temperature.

A plot of the fiber draw velocity (y axis) versus input parameter uncertainty in terms of the coefficient of variance, σ/μ (x axis), is shown in Figure 3. This is to study the effect of uncertainty on the fiber draw velocity. The constraint on the average refractive index profile error is kept constant at 7.5%, while the constraint on the maximum refractive index profile error is varied at 15.0%, 17.5%, and 20.0%. $\sigma/\mu = 0$ refers to the case without uncertainty (nominal optimization). It is observed that the fiber draw speed decreases very rapidly (nonlinearly) with an increase in uncertainty.

As observed earlier, from the sensitivity analysis, it was found that an increase in the furnace wall temperature affects all the output variables. The consequence here is that most of the constraints in the optimization problem are violated. Only the

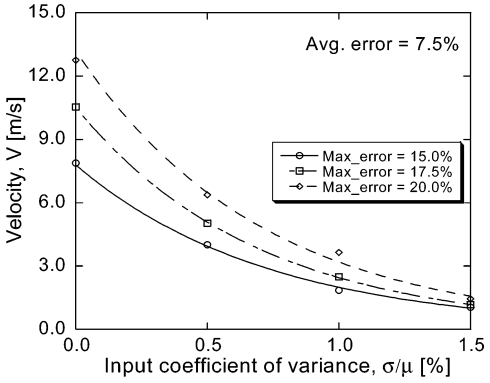

Figure 3. Plot of fiber velocity versus level of uncertainty for various maximum refractive index profile errors (σ/μ = 0.5%, 1.0%, and 1.5%).

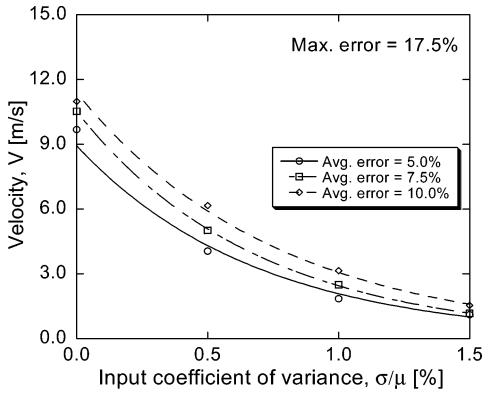

Figure 4. Plot of fiber velocity versus level of uncertainty for various average refractive index profile errors (σ/μ = 0.5%, 1.0%, and 1.5%).

drawing tension constraint reduces with an increase in temperature. Therefore, as uncertainty increases, a decrease in temperature (reduced temperature gradients) is necessary to ensure that constraints are satisfied. This reduction in temperature results in reduced flow, since the preform becomes more viscous. Consequently, the fiber draw velocity decreases.

Figure 4 shows a similar plot to that of Figure 3. However, in Figure 4, the constraint on the maximum refractive index profile error is kept constant at 17.5%, while the constraint on the average refractive index profile error is varied at 5.0%, 7.5%, and 10.0%. Here also, it is seen that the fiber draw velocity decreases very rapidly as the level of uncertainty increases.

The effect of constraint on the maximum and average index of refraction profile error on the fiber draw velocity was also investigated and is explained using Figures 3 and 4. Figure 3 shows the effect of the maximum refractive index profile error constraint on the fiber draw velocity. It can be observed that, for a fixed level of uncertainty, the draw velocity increases as constraints become more relaxed from 15.0% through 17.5% and then to 20.0%. An increase in maximum refractive index profile error is undesirable, as this leads to marked deviations of the actual refractive index profile from the reference profile. To minimize this effect, a much tighter constraint is required (e.g., maximum error = 10.0%), but this can be achieved at considerably low draw speeds, which directly reduces the rate of production. The effect of the average refractive index profile error constraint on the fiber draw velocity is shown in Figure 4. Here also, it is observed that, for a fixed input coefficient of variance, the fiber draw velocity increases as the average refractive index profile error is relaxed from 5.0% through 7.5% to 10.0%.

Plots of the normalized optimal value of design variable, $\bar{\Theta}$, versus uncertainty level are shown in Figures 5−9. The

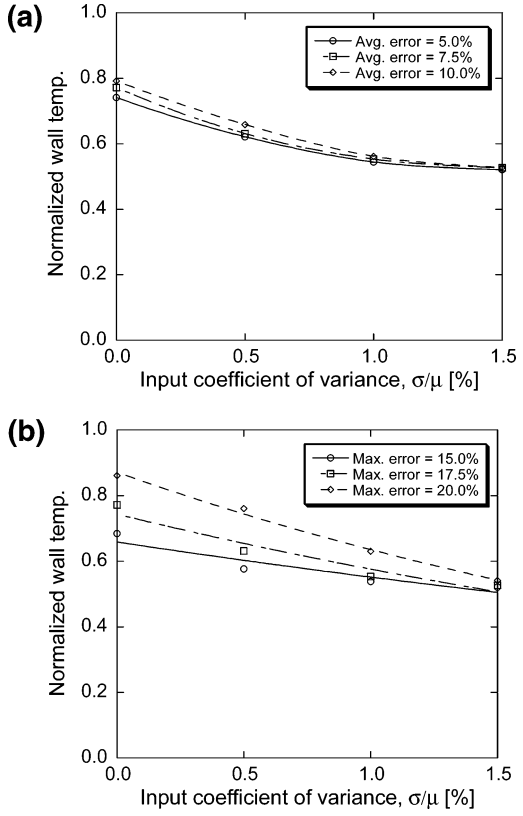

Figure 5. (a) Normalized wall temperature versus uncertainty level for various average refractive index profile errors. (b) Normalized wall temperature versus uncertainty level for various maximum refractive index profile errors.

normalized variable is calculated as

$$\bar{\Theta} = \frac{\mathbf{d}_i - \mathbf{d}_{i,\min}}{\mathbf{d}_{i,\max} - \mathbf{d}_{i,\min}}, \quad i = 1, ..., 6 \tag{29}$$

where $\mathbf{d}_i$ represents the actual value of the design variable at the end of the optimization run. $\mathbf{d}_{i,\min}$ and $\mathbf{d}_{i,\max}$ represent, respectively, the lower and upper bounds on the design variable used in the optimization.

A plot of normalized wall temperature versus input coefficient of variance is shown in parts a and b of Figure 5. Figure 5a shows the case for which the constraint on the maximum refractive index profile error is kept constant at 17.5%, while the constraint on the average refractive index profile error is varied at 5.0%, 7.5%, and 10.0%. In Figure 4b, the constraint on the average refractive index profile error is fixed at 7.5%, while the constraint on the maximum refractive index profile error is varied at 15.0%, 17.5%, and 20.0%. The observation in both plots is that the wall temperature decreases with increasing uncertainty.

The plots for the normalized initial dopant concentration versus input coefficient of variance are shown in parts a and b of Figure 6. Neither plot reveals any clear pattern. Since the range for the scaled variables is from 0 to 1, it can be inferred that low levels of initial dopant concentration are generally preferred in the fiber drawing process.

Parts a and b of Figure 7 show the plots of normalized cooling disk temperature versus level of uncertainty. The cooling disk temperature is observed to decrease with an increase in uncertainty. However, for a fixed level of uncertainty, the value of the cooling disk temperature does not change very much as the constraints on the average index of refraction profile error

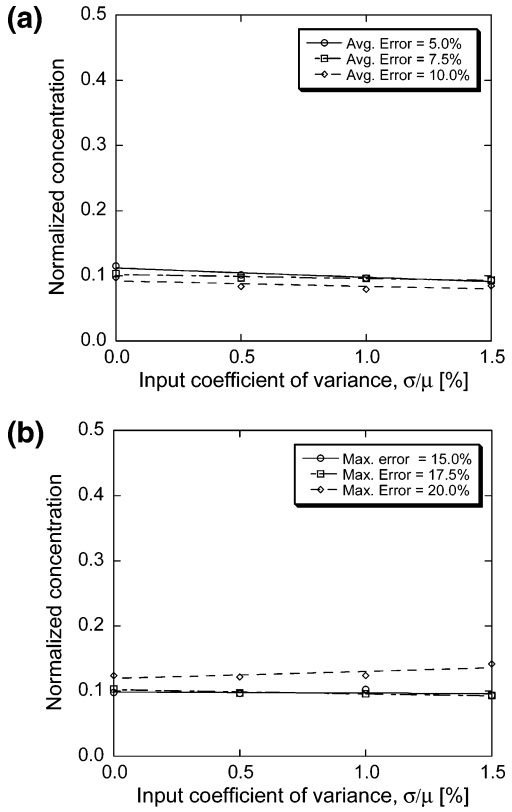

Figure 6. (a) Normalized concentration versus uncertainty level for various average refractive index profile errors. (b) Normalized concentration versus uncertainty level for various maximum refractive index profile errors.

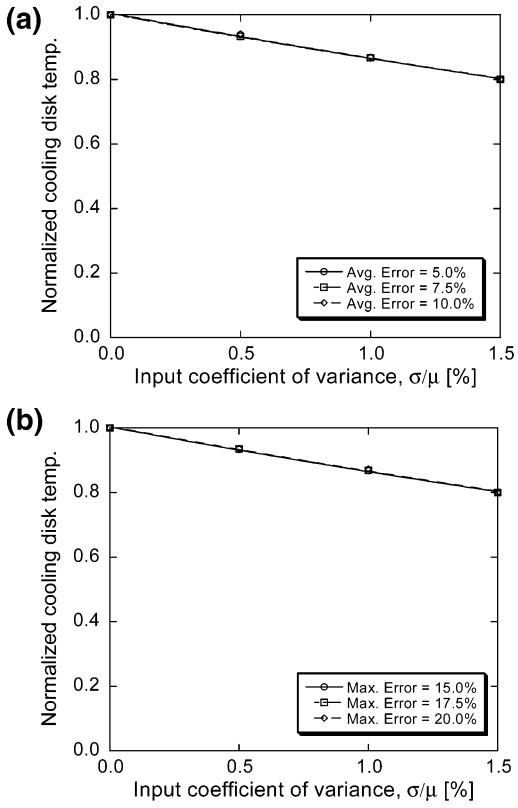

Figure 7. (a) Normalized disk temperature versus uncertainty level for various averate refractive index profile errors. (b) Normalized disk temperature versus uncertainty level for various maximum refractive index profile errors.

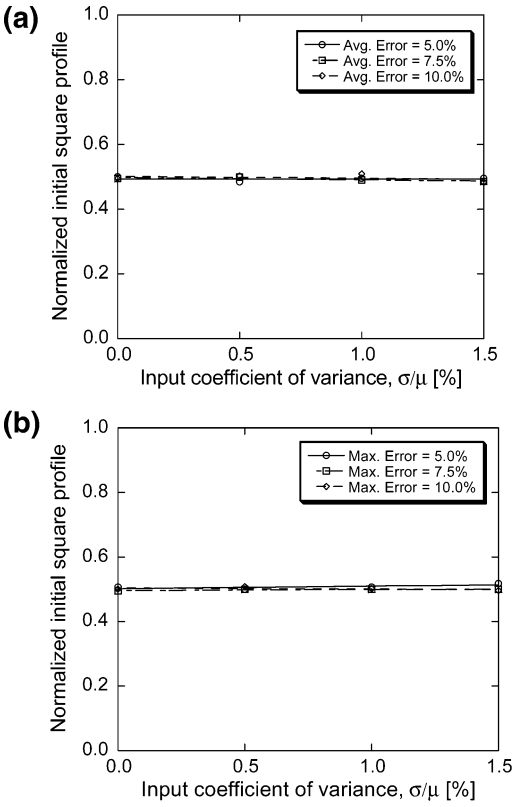

Figure 8. (a) Normalized initial sq. profile versus uncertainty level for various average refractive index profile errors. (b) Normalized initial sq. profile versus uncertainty level for various maximum refractive index profiles.

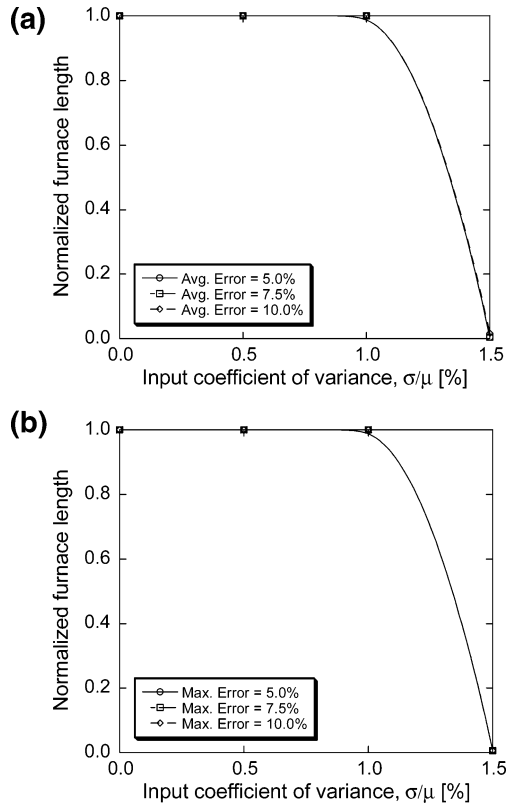

Figure 9. (a) Normalized furnace length versus uncertainty level for various average refractive index profile errors. (b) Normalized furnace length versus uncertainty level for various maximum refractive index profile errors.

and maximum index of refraction profile error are varied. The cooling disk temperature, therefore, affects the fiber drawing process only to a small extent, as shown earlier on using the sensitivity analysis.

Parts a and b of Figure 8 show plots of the normalized initial square profile versus level of uncertainty. It is evident from both plots that the trend is almost horizontal; hence, the optimized value is ~0.5 at all uncertainty levels. In parts a and b of Figure 9, the furnace length is at its upper bound for $\sigma/\mu = 0.5\%$ and $\sigma/\mu = 1.0\%$, respectively. However, the furnace length decreases sharply to its lower bound value at $\sigma/\mu = 1.5\%$. As observed earlier, an increase in uncertainty necessitates a reduction in temperature, which is achieved only when the molten preform stays in the furnace for a shorter time (shorter residence time). A longer residence time implies a high-temperature rise, resulting in large temperature gradients and constraint violation.

6. Summary and Conclusions

The effect of uncertainty on the optical fiber manufacturing process has been studied, and the results are summarized as follows:

- The fiber draw velocity decreases with an increase in the uncertainty level. Since the velocity is directly related to the production throughput, it means the overall production throughput decreases with an increase in uncertainty.
- At a fixed level of uncertainty, the velocity and, hence, the production throughput decrease as the maximum index of refraction profile error decreases. Also, as the average refractive index profile error constraint decreases, the velocity decreases.
- An increase in the level of uncertainty results in a decrease in the wall temperature.
- The furnace wall temperature is found to be the most important decision variable in the fiber drawing problem since it affects all thermophysical properties such as diffusion, viscosity, and radiation coefficients. It is, therefore, crucial to keep temperature fluctuations to the barest minimum in the fiber drawing process. This will require that a very good temperature-control system be put in place.
- The cooling disk temperature decreases with uncertainty only to a small extent.
- Higher uncertainty levels ($\sigma/\mu = 1.5\%$) necessitate reduction in the furnace length.

Acknowledgment

This material is based on work supported by the National Science Foundation under Grant No. CTS 0112822. Any opinions, findings, and conclusions or recommendations expressed in this material are those of the authors and do not necessarily reflect the views of the National Science Foundation. The authors also acknowledge Dr. Yonghong Yan for developing the optical fiber drawing code used in the study.

Nomenclature

A = cross-sectional area of fiber core (m^2)
c = dopant concentration expressed as mass fraction
C = dimensionless dopant concentration
C_p = specific heat (kJ kg^{-1} K^{-1})
D = diffusion coefficient (m^2 s^{-1})
D_0 = inert diffusion constant 1 (m^2 s^{-1})
D_1 = inert diffusion constant 2 (K)
h = heat transfer coefficient for natural convective cooling (W m^{-2} K^{-1})
k_{cond} = thermal conductivity (W m^{-1} K^{-1})
R = radius of fiber core (m)
T = temperature in absolute scale (K)
u = axial velocity component (m s^{-1})
v = axial velocity component (m s^{-1})
z = axial coordinate (m)
V = fiber draw speed (m s^{-1})
V_η = viscosity coefficient (Ns m^{-2})

Greek Symbols

ϵ = sufficiently small and positive scalar
σ/μ = input uncertainty coefficient of variance (dimensionless)
η = dynamic viscosity (Ns m^{-2})
ρ = density (kg m^{-3})
$\boldsymbol{\theta}$ = uncertain parameter vector
Θ = normalized variable

Subscripts

avg = average value
crit = critical value
def = defects
max = maximum value
min = minimum value
tens = tension

Literature Cited

(1) Rooney, W. C.; Biegler, L. T. Incorporating joint confidence regions into design under uncertainty. *Comput. Chem. Eng.* **1999**, *23*, 1563−1575.

(2) Acevedo, J.; Pistikopoulos, E. N. A multiparametric programming approach for linear process engineering problems under uncertainty. *Ind. Eng. Chem. Res.* **1997**, *36*, 717−728.

(3) Bhatia, T. K.; Biegler, L. T. Multiperiod design and planning with interior point methods. *Comput. Chem. Eng.* **1999**, *23*, 919−932.

(4) Dua, V.; Pistikopoulos, E. N. An algorithm for the solution of multiparametric mixed integer linear programming problems. *Ann. Oper. Res.* **2000**, *99*, 123−139.

(5) Halemane, K. P.; Grossmann, I. E. Optimal process design under uncertainty. *AIChE J.* **1983**, *29*, 425−433.

(6) Ostrovski, G. M.; Volin, Y. M.; Senyavin, M. M. An approach to solving a two-stage optimization problem under uncertainty. *Comput. Chem. Eng.* **1997**, *21*, 317−325.

(7) Ostrovski, G. M.; Achenie, L. E. K.; Wang, Y.; Volin, Y. M. A new algorithm for computing process flexibility. *Ind. Eng. Chem. Res.* **2000**, *39*, 2368−2377.

(8) Pistikopoulos, E. N.; Ierapetritou, M. G. A novel approach for optimal process design under uncertainty. *Comput. Chem. Eng.* **1995**, *19*, 1089−1110.

(9) Rooney, W. C.; Biegler, L. T. Design for model parameter uncertainty using nonlinear confidence regions. *Comput. Chem. Eng.* **2001**, *47* (8), 1794−1804.

(10) Varvarezos, D. K.; Grossmann, I. E.; Biegler, L. T. A sensitivity based approach for flexibility analysis and design of linear process systems. *Comput. Chem. Eng.* **1995**, *19*(12), 1301−1316.

(11) Ostrovski, G. M.; Achenie, L. E. K.; Datskov. I.; Volin, Y. M. Uncertainty at both design and operation stage. *Chem. Eng. Commun.* **2004**, *191*, 105−124.

(12) Kirchhof, J.; Kleinert, P.; Funke, A.; Knappe, B.; Muller, H. R. About the smoothing of concentration fluctuations by diffusion in the glass systems SiO_2/GeO_2 and $SiO_2/GeO_2/B_2O_3$. *Cryst. Res. Technol.* **1987**, *22*, K105−K108.

(13) Paek, U. C.; Runk, R. B. Physical behavior of the neck-down region during furnace drawing of silica fibers. *J. Appl. Phys.* **1978**, *49*, 4417−4422.

(14) Paek, U. C.; Schroeder, C. M. Forced convective cooling of optical fibers in high-speed coating. *J. Appl. Phys.* **1979**, *50*, 6144−6148.

(15) Kaminski, D. A. Thermal transport in optical fiber manufacturing. *Proc. First Int. Symp. Radiat. Transfer* **1995**, 667−681.

(16) Lee, S. H.-K.; Jaluria, Y. The effect of geometry and temperature variations on the radiative transport during optical fiber drawing. *J. Mater. Process. Manuf. Sci.* **1995**, *3*, 317−331.

(17) Lee, S. H.-K.; Jaluria, Y. Effects of variable properties and viscous dissipation during optical fiber drawing. *ASME J. Heat Transfer* **1996**, *118*, 350−358.

(18) Issa, J.; Yin, Z.; Polymeropoulos, C. E.; Jaluria, Y. Temperature distribution in an optical fiber draw tower furnace. *J. Mater. Process. Manuf. Sci.* **1996**, *4*, 221−232.

(19) Goseaux, M. G.; Bourhis, J. F.; Orce, G. Numerical simulation of optical fiber cooling during the fiber drawing process. *Int. Wire Cable Symp. Proc.* **1998**, 81−84.

(20) Vaidya, D. S.; Mihalacopoulos, G. D. Characterization of meltdown profile during fiber draw. *Int. Wire Cable Symp. Proc.* **1998**, 73−80.

(21) Paek, U. C. Fiber drawing and polymer coating of silica glass optical fibers. *ASME J.* **1999**, *121*, 774−788.

(22) Koaizawa, H.; Orita, N.; Kamiya, T. Study of coating diameter at high-speed drawing of optical fibers with UV curable resin. *Tech. Dig. IOOC'95* **1995**, *4* (FA1-2), 4−5.

(23) Kobayashi, K.; Tsurusaki, K.; Sata, Y.; Araki, S. High-speed coating of optical fibers with UV curable resins. *Int. Wire Cable Symp. Proc.* **1991**, 126−133.

(24) Chida, K.; Sakaguchi, S.; Wagatsuma, M.; Kimura, T. High-speed coating of optical fibers with thermally curable silicon resin using a pressure die. *Electron Lett.* **1982**, *18*, 713−715.

(25) Paek, U. C.; Schroeder, C. M. High-speed coating of optical fibers with UV curable materials at a rate greater than 5 m/s. *Appl. Opt.* **1981**, *20*, 330−335.

(26) Paek, U. C.; Schroeder, C. M. Calculation of photopolymerization energy required for optical fiber coating. *Appl. Opt.* **1981**, *20*, 1230−1233.

(27) Yan, Y.; Pitchumani, R. Numerical study on the dopant concentration and refractive index profile evaluation in an optical fiber manufacturing process. *Int. J. Heat Mass Transfer* **2006**, in press.

(28) Hanafusa, H.; Hibino, Y.; Yamamoto, F. Formation mechanism of drawing-induced E centers in silica optical fibers. *J. Appl. Phys.* **1985**, *58* (3), 1356−1361.

(29) Paek, U. C.; Kurkjian, C. R. Calculation of cooling rate and induced stresses in drawing of optical fibers. *J. Am. Ceram. Soc.* **1975**, *58*, 330−335.

(30) Kurkjian, C. R.; Paek, U. C. Effect of drawing tension on residual stresses in clad glass fibers. *J. Am. Ceram. Soc.* **1978**, *61*, 176−177.

(31) Hibino, Y.; Hanawa, F.; Horiguchi, M. Drawing-induced residual stress effects on optical characteristics in pure-silica-core single-mode fibers. *J. Appl. Phys.* **1989**, *65*, 30−34.

(32) Pistikopoulos, E. N.; Mazzuchi, T. A. A novel flexibility analysis approach for processes with stochastic parameters. *Comput. Chem. Eng.* **1990**, *14*, 991−1000.

(33) Straub, D. A.; Grossmann, I. E. Design optimization of stochastic flexibility. *Comput. Chem. Eng.* **1993**, *17*, 339−354.

(34) Pai, C. D.; Hughes, R. R. Strategies for formulating and solving two-stage problems for process design under uncertainty. *Comput. Chem. Eng.* **1987**, *11*, 695−706.

(35) Chadhuri, P. D.; Diwekar, U. M Process synthesis under uncertainty: A penalty function approach. *AIChE J.* **1996**, *42*, 742−752.

(36) Pistikopoulos, E. N.; Ierapetritou, M. G. A novel approach for optimal process design under uncertainty. *Comput. Chem. Eng.* **1995**, *19*, 1089−1110.

(37) Liu, M. L.; Sahinidis, N. V. Optimization in process planning under uncertainty. *Ind. Eng. Chem. Res.* **1996**, *35*, 4154−4165.

(38) Padmanabhan, S. K.; Pitchumani, R. Stochastic analysis of isothermal cure of resin systems. *Polym. Compos.* **1999**, *20*, 72−85.

(39) Padmanabhan, S. K.; Pitchumani, R. Stochastic analysis of nonisothermal flow during resin transfer molding. *Int. J. Heat Mass Transfer* **1999**, *42*, 3057−3070.

(40) Mawardi, A.; Pitchumani, R. Cure cycle design for thermosetting-matrix under uncertainty. *Ann. Oper. Res.* **2004**, *132*, 19−45.

(41) Grossmann, I. E.; Sargent, R. W. H. Optimum design of chemical plants with uncertain parameters. *AIChE J.* **1978**, *24*, 1021−1028.

(42) Halemane, K. P.; Grossmann, I. E. Optimal process design under uncertainty. *AIChE J.* **1983**, *29*, 425−433.

(43) Varvarezos, D. K.; Grossmann, I. E.; Biegler, L. T. An outer-approximation method for multiperiod design optimization. *Ind. Eng. Chem. Res.* **1992**, *31*, 1466−1477.

(44) Ostrovsky, G.; Achenie, L. E. K.; Datskov, I.; Volin, Y. Optimization of chemical processes under uncertainty: The case of insufficient process data at the operation stage. *AIChE J.* **2003**, *49*, 1216−1232.

(45) Ostrovski, G. M.; Achenie, L. E. K.; Datskov. I.; Volin, Y. M. Uncertainty at both design and operation stage. *Chem. Eng. Commun.* **2004**, *191*, 105−124.

(46) Choudhury, S. R.; Jaluria, Y.; Vaskopoulos, T.; Polymeropoulos, C. E. Forced convective cooling of optical fiber drawing process. *ASME J. Heat Transfer* **1994**, *116*, 790−794.

(47) Choudhury, S. R.; Jaluria, Y. Thermal transport due to material and gas flow in a furnace for drawing an optical fiber. *J. Mater. Res.* **1998**, *13* (2), 494−503.

(48) Iman, R. L.; Shortencarier, M. J. *A FORTRAN77 program and user's guide for generation of Latin Hypercube and random samples for use with computer models*; Technical Report, 1984, NUREG/CR-3624, SAND83-2365; Sandia National Laboratories: Alberquerque, NM.

Received for review January 11, 2006
Revised manuscript received April 7, 2006
Accepted April 11, 2006

IE060045U